Available online at www.sciencedirect.com
ScienceDirect
Journal of the European Ceramic Society 30 (2010) 2155–2164
www.elsevier.com/locate/jeurceramsoc

Toughened ZrB_2-based ceramics through SiC whisker or SiC chopped fiber additions

Laura Silvestroni *, Diletta Sciti, Cesare Melandri, Stefano Guicciardi

ISTEC-CNR, Via Granarolo 64, I-48018 Faenza (RA), Italy

Available online 16 December 2009

Abstract

In order to improve the fracture toughness, SiC whiskers or SiC chopped fibers were added to a ZrB_2 matrix in volumetric fraction of 10 and 20 vol.%. The composites were hot-pressed between 1650 and 1730 °C and their final relative densities were higher than 95%. Even at the lowest sintering temperature, the whiskers showed an evident degradation. On the other hand, the fibers maintained their initial shape and a strong interface formed between matrix and reinforcement. The fracture toughness of the composites increased from 30 to 50% compared to the baseline material, with the fibers showing a slightly higher toughening effect. In the whiskers-reinforced composites, the room-temperature strength increased when 10 vol.% whiskers were added. In the fibers-reinforced composites, the room-temperature strength decreased regardless the amount of fibers added. The high-temperature strength of the composites was higher than that of the baseline material for both types of reinforcement.

Keywords: ZrB_2; Whiskers; Fibers; Microstructure; Fracture toughness

1. Introduction

Among the so-called ultra high-temperature ceramics (UHTCs), ZrB_2-based materials are of particular interest because of their combination of suitable properties such as high melting point, relatively low density, high mechanical resistance and hardness. These properties make them adequate for high-temperature uses in refractory industry and especially in aerospace field, as components in hypersonic re-entry vehicles.

It has been widely proved that the addition of SiC further improves the fracture strength and the oxidation resistance of the ZrB_2-based composites due to the grain refinement and the formation of a protective silica-based protective layer, respectively.[1,2] So far, many efforts have been done on ZrB_2–SiC composites in order to improve the mechanical properties and oxidation performances, however, the poor fracture toughness, around 2–5 MPa $m^{1/2}$, is still limiting the spectrum of potential applications.[3–5]

In some preliminary works,[6–10] it has been reported that the addition of whiskers, short fibers, or nanotubes gives promising results. For ZrB_2-based composites, fracture toughness values up to 6.6–8.5 MPa $m^{1/2}$ were reported by single edge notched beam (SENB). [6–10]

The attempts realized so far pointed out that some critical parameters, like the dimension and purity of the starting phases, the mixing procedure and the sintering temperatures are still to be optimized in order to avoid the degeneration of elongated reinforcements into particles,[7] their agglomeration[10] or breaking.[11] However, these first experiments open a window on the concrete possibility of increasing the fracture toughness of UHTCs by correctly tuning the aforementioned parameters.

Hence, to achieve high toughness values using fiber or whisker additions, three major obstacles have to be overcome: a difficult dispersion in the matrix due to the high aspect ratio, the degradation of the reinforcing elements at high temperature and the development of a strong interface after reaction with the matrix.

In the current paper we present the microstructure and the mechanical properties of ZrB_2–5 vol.% Si_3N_4 materials reinforced with 10 and 20 vol.% of SiC whiskers or SiC chopped fibers. They were mainly produced with the aim to improve the fracture toughness of the matrix, however the effect of the reinforcement on the fracture strength was also evaluated.

2. Experimental procedure

The compositions under investigation are indicated in Table 1. Commercial powders were used to prepare the ceramic composites: hexagonal ZrB_2 Grade B (H.C. Starck,

* Corresponding author. Tel.: +39 0546 699723; fax: +39 0546 46381.
E-mail address: laura.silvestroni@istec.cnr.it (L. Silvestroni).

0955-2219/$ – see front matter © 2009 Elsevier Ltd. All rights reserved.
doi:10.1016/j.jeurceramsoc.2009.11.012

Table 1
Composition, sintering parameters of the hot-pressed samples. T_{ON}: temperature at which the shrinkage started and T_{MAX}: temperature held for the dwell time.

Label	Composition (vol.%)	T_{ON} (°C)	T_{MAX} (°C)	Dwell time (min)	Th. density (g/cm^3)	Final density (g/cm^3)	Rel. density (%)
ZB	$ZrB_2 + 5Si_3N_4$	1580	1700	15	5.95	5.89	99.0
ZB10w	ZB + 10SiCw	1590	1730	11	5.57	5.45	97.9
ZB20w	ZB + 20SiCw	1545	1650	10	5.28	4.89	94.0
ZB10f	ZB + 10SiCf	1625	1730	11	5.53	5.42	97.8
ZB20f	ZB + 20SiCf	1560	1700	10	5.22	5.07	97.0

Germany), specific surface area 1.0 m^2/g, impurity max content: C: 0.25 wt%, O: 2 wt%, N: 0.25 wt%, Fe: 0.1 wt%, Hf: 0.2 wt%, particle size range 0.1–8 μm; α-Si_3N_4 Baysind (Bayer, Germany), specific surface area 12.2 m^2/g, impurity max content: O: 1.5 wt%; SiC chopped fibers (HI Nicalon) diameter: 14 μm, length: 1 mm, 1–5 wt% vinyl alcohol polymer with vinyl acetate wt% Si:C:O = 62:37:0.5. For SiC whiskers no data sheet was available, the dimensions calculated by image analysis were diameter: 1 μm and length: 30 μm. The starting whiskers and chopped fibers utilized for the composites are shown in Fig. 1a and b.

The powder mixtures were ball milled for 24 h in absolute ethanol using silicon carbide media. Subsequently, the slurries were dried in a rotary evaporator. After mixing, SEM analysis showed that the fibers length was reduced to about 400 μm, as can be observed in Fig. 1c and d. Hot-pressing cycles were conducted in low vacuum (∼100 Pa) using an induction-heated graphite die with an uniaxial pressure of 30 MPa during the heating and increased up to 50 MPa at 1650 °C, for the material containing 20 vol.% of whiskers, and at 1700 °C for the other composites. The maximum sintering temperature was set on the basis of the shrinkage curve. Free cooling followed. The schedule of each sintering runs is reported in Table 1.

The bulk densities were measured by Archimedes' method. Crystalline phases were identified by X-ray diffraction (Siemens D500, Germany). The microstructural features were analyzed on the fractured and polished surfaces using scanning electron microscopy (SEM, Cambridge S360, Cambridge, UK) and energy-dispersive spectroscopy (EDS, INCA Energy 300, Oxford instruments, UK).

TEM specimen preparation was quite difficult, because whiskers and fibers tend to fall during ion milling procedure due to the high aspect ratio. Unfortunately, specimens of the hot-pressed composites did not survive the ion thinning process, hence in this work TEM analysis on the same powder mixtures sintered by SPS will be presented, as we believe that no substantial difference exists between the final microstructures after hot pressing or spark plasma sintering.[12] TEM samples were prepared by cutting 3 mm discs from the sintered pellets. These were mechanically ground down to about 15 μm and then

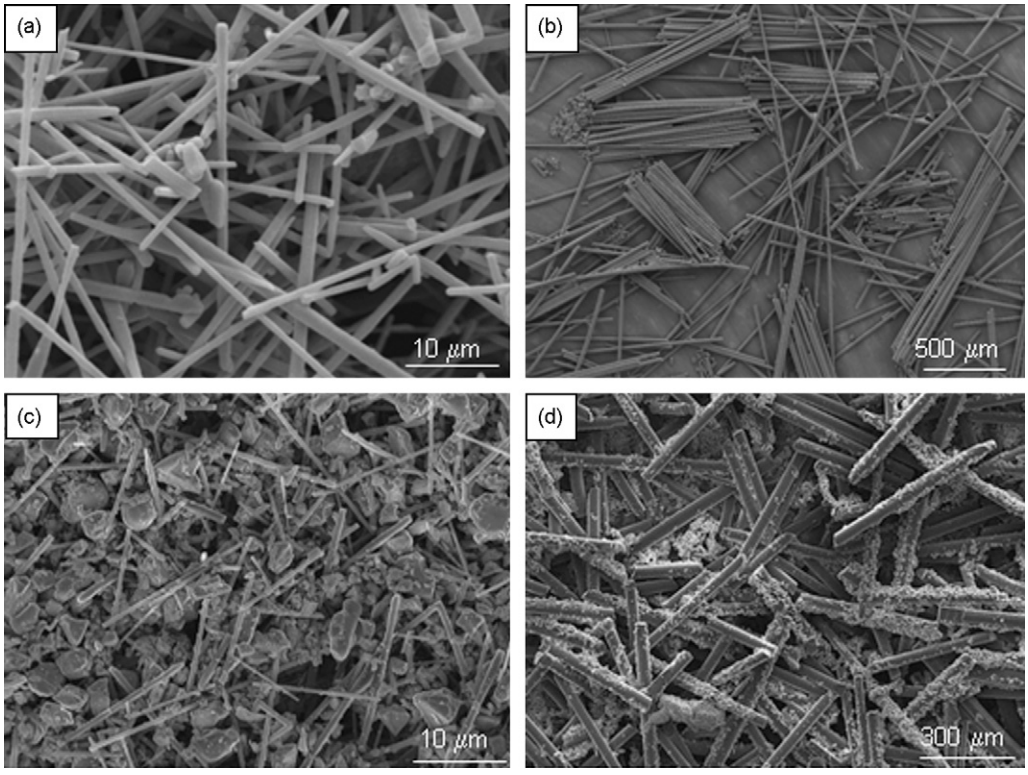

Fig. 1. Reinforcing phases added to the ZrB_2 matrix: (a) SiC whiskers and (b) Hi Nicalon SiC chopped fibers. The powder mixtures before sintering: (c) ZB20w and (d) ZB20f.

further ion beam thinned until small perforations were observed by optical microscopy. Local phase analysis was performed using transmission electron microscopy (TEM) equipped with an energy-dispersive X-ray system (FEI, CM12, Eindhoven, The Netherlands; EDS, EDAX Genesis 2000, Ametek GmbH; Wiesbaden, Germany) operating at a nominal voltage of 120 keV. High-resolution investigations were performed using a FEI CM20 STEM operating at a nominal voltage of 200 keV.

The sintering cycle for the spark plasma sintered specimens was adopted as follows. The samples were heated to 600 °C at a rate of 300 °C/min, to the sintering temperature at 100 °C/min. The sample containing whiskers was sintered at 1600 °C for 3 min under 75 MPa, the one containing fibers at 1500 °C for 5 min under 100 MPa. Further details on these SPSed samples will be the object of future works.

Vickers microhardness (HV1.0) was measured with a load of 9.81 N, using a Zwick 3212 tester. The fracture toughness (K_{Ic}) was evaluated using chevron-notched beams (CNB) in flexure. The test bars, 25 mm × 2 mm × 2.5 mm (length by width by thickness, respectively), were notched with a 0.1-mm thick diamond saw; the chevron-notch tip depth and average side length were about 0.12 and 0.80 of the bar thickness, respectively. The specimens were fractured using a semi-articulated silicon carbide four-point fixture with a lower span of 20 mm and an upper span of 10 mm using a screw-driven load frame (Instron mod. 6025). The specimens were loaded with a crosshead speed of 0.05 mm/min. The "slice model" equation of Munz et al.[13] was used to calculate K_{Ic}. On the same machine and with the same fixture, the flexural strength (σ) was measured at room-temperature and at 1200 °C in air. For each material and temperature, at least five bars were tested. The interaction of the crack front with the microstructure was analyzed by introducing cracks onto polished surfaces with a 10-kg indentation.

3. Results and discussion

3.1. Densification

Since the reinforcing phases tend to degenerate during thermal treatment, the sintering temperature must be kept as low as possible. For this purpose, Si_3N_4 was selected as sintering aid as it promotes the full densification of ZrB_2 at 1700 °C.[14]

The densification curves recorded during the hot-pressing cycles for each composite are reported in Fig. 2. The reinforced ceramics were sintered at temperatures from 1650 to 1730 °C, as shown in Table 1. As the introduction of elongated reinforcement is thought to hinder the shrinkage, the applied pressure was increased from 30 to 50 MPa when the temperature reached 1700 or 1650 °C as indicated by the small shoulder in the curves (indicated by arrows in Fig. 2). For the composites containing 20 vol.% of reinforcement, temperatures of 1650 and 1700 °C let the achievement of a relative density of 94 and 97% when whiskers or fibers were employed, respectively. As for the baseline material, the sudden increase of the densification rate, which occurred at 1545–1630 °C, indicates the activation of the mass transfer mechanisms through the formation of a liquid phase.

The final relative densities were expressed as the ratio of experimental and theoretical values calculated with the rule

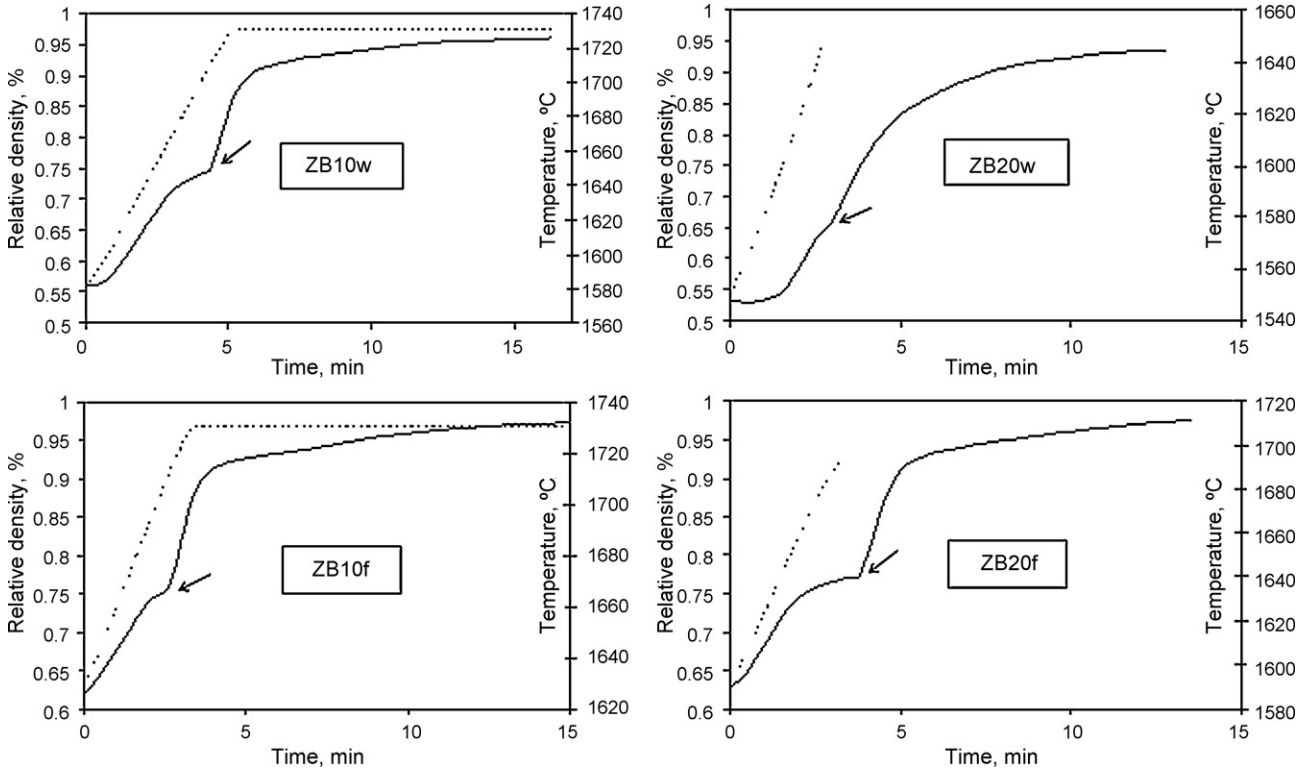

Fig. 2. Densification curves recorded during hot-pressing cycles of the reinforced composites (see Table 1 for the definition of the labels). The continuous line represents the relative density as a function of the time, the dotted line the temperature as a function of the time. The arrows indicate the increase of pressure from 30 to 50 MPa.

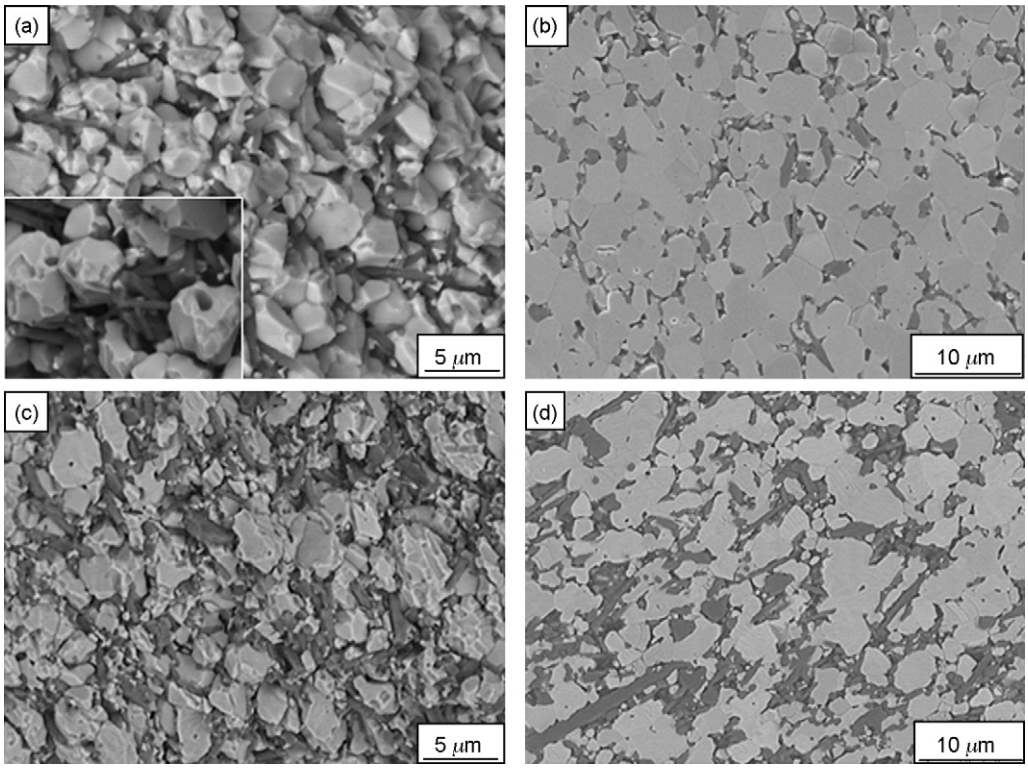

Fig. 3. Fracture and polished surfaces for (a) and (b) ZB10w; (c) and (d) ZB20w. The surface normal to the applied pressure direction is shown. In the inset in (a), some whiskers pullout is put in evidence.

of mixture considering the starting compositions and taking 5.95 g/cm^3 as the density of baseline material, 3.20 g/cm^3 and 2.73 g/cm^3 for the whiskers and fibers density, respectively. As can be seen in Table 1, with the exception of ZB20w, the relative densities were higher than 97%. Furthermore, these values can be still underestimated due to significant amounts of glassy phase formed by reaction of the matrix with Si_3N_4 and the reinforcement, as illustrated later.

3.2. Microstructure

The baseline ZrB_2 material doped with 5 vol.% of Si_3N_4 was fully dense with a mean grain size around 2.7 μm. The secondary phases observed in the sintered microstructure were mainly concentrated at triple points and were identified as ZrO_2, BN, Zr–Si phases, discrete pockets of SiO_2 and a borosilicatic glass containing Zr–Si–B–N–O. More microstructural details of the baseline material are reported in Ref. [15][15].

The fractured and polished sections of the whiskers-reinforced composites are reported in Fig. 3. As it can be seen, porosity is not so apparent in the fractured surfaces; only some small pores trapped into the ZrB_2 grains can be observed, especially in the sample containing 20 vol.% of whiskers. In the inset of Fig. 3a, some whisker pullout is evidenced. The whiskers were generally well dispersed into the matrix, still recognizable as elongated dark structure in back-scattered SEM images (Fig. 3b and d). After sintering, the whiskers assumed a squatter aspect with irregular edges. On the polished surface, diffused microcracking was observed, as reported for the baseline material,[13] due to the mismatch of thermal coefficients and elastic constants among ZrB_2, SiC and the newly formed glassy phase. At higher magnification, the presence of ZrO_2 agglomerates on the SiC and Zr–Si phases was confirmed, together with a Zr–Si–B–N glassy phase which surrounded the whiskers (see Fig. 4). Transmission electron microscopy (TEM) analyses carried out on the same compositions sintered by spark plasma sintering (SPS) evidenced a Zr–Si–B–N amorphous intergranular layer, crystalline $ZrSi_2$ at the triple point junctions and BN as intergranular pockets. The interface between matrix and whiskers was wet by the same intergranular phase, as depicted in Fig. 5. We believe that the composites object of this paper, sintered by hot pressing, do not present significant microstructural differences from the just mentioned composites sintered by spark plasma sintering.

The fractured and polished sections of the fibers-reinforced composites are reported in Fig. 6. Also in this case the dispersion of the fibers into the matrix was homogeneous, since no agglomeration was observed. Porosity was nearly absent and the microcracking was apparently less pronounced compared to the whisker-reinforced composites. As expected, the fibers showed a strong tendency to align their long axis perpendicular to the direction of applied pressure The length of the fibers was further reduced from the starting mixture, due to both the action of the milling media and the applied pressure during sintering. On the fracture surfaces, no trace of fiber pullout was observed. During densification, a Zr–Si–C–O-based interface formed between the matrix and the SiC fibers due to the SiC/ZrB_2 interaction (Fig. 7). By TEM analysis on analogous compositions sintered by SPS, the stoichiometry of the

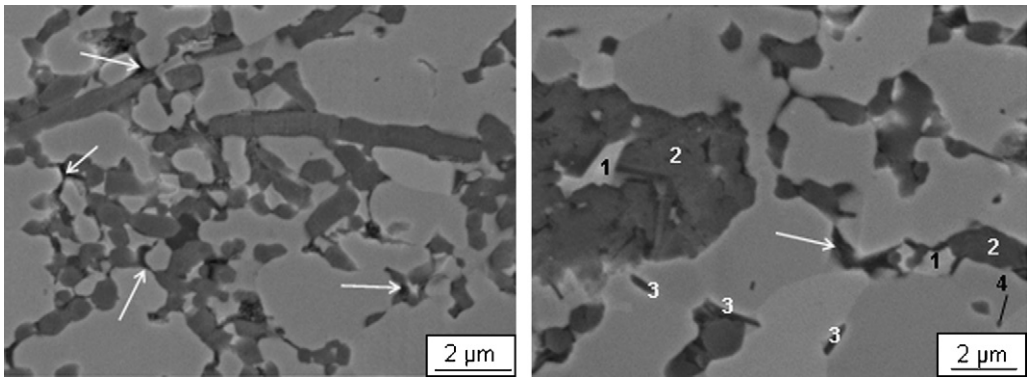

Fig. 4. Examples of microstructure of the whiskers-reinforced composites. Note the glassy phase indicated by arrows and the secondary phases: (1) ZrO_2, (2) SiC, (3) BN, and (4) $ZrSi_2$.

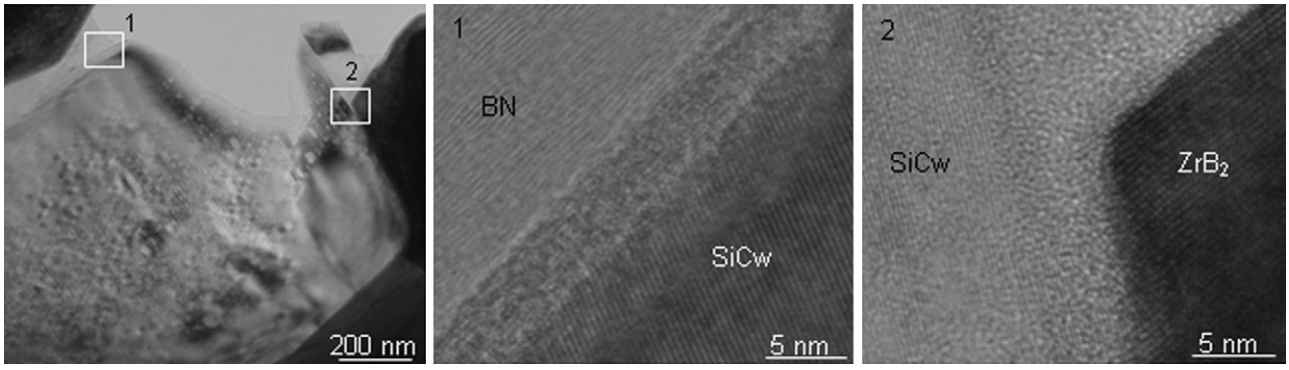

Fig. 5. BF-TEM images showing the interfaces between SiC whiskers and BN or ZrB_2 (left). To the right, the HRTEM images of the insets showing an amorphous interlayer surrounding the whiskers.

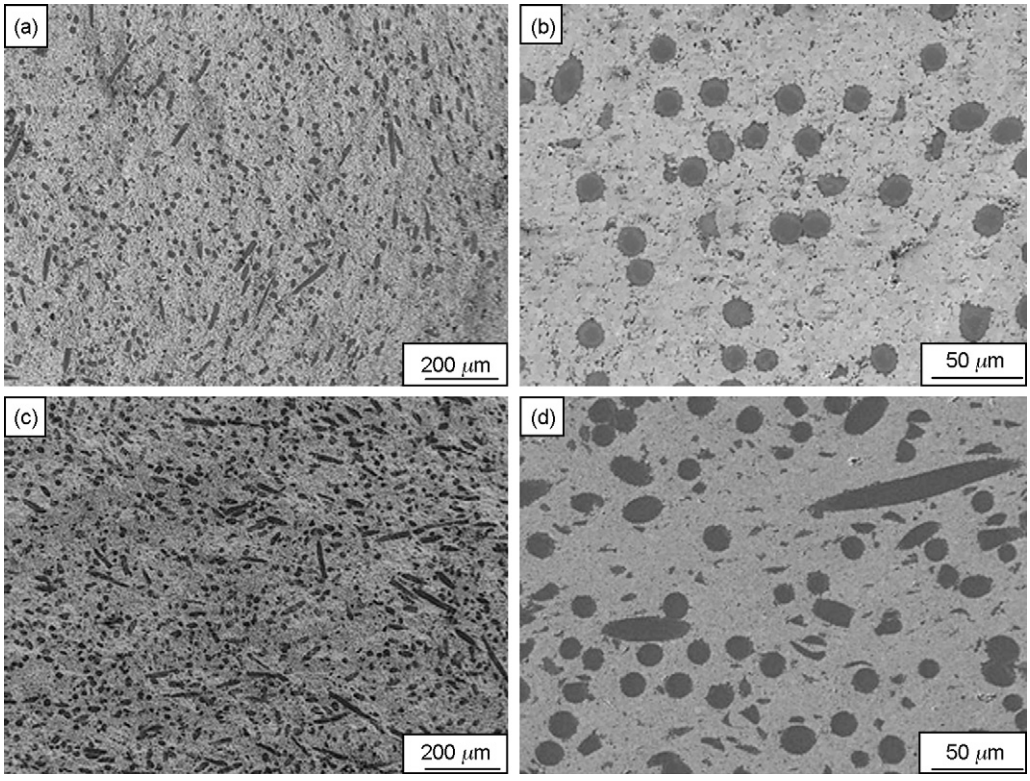

Fig. 6. Fracture and polished surfaces for (a) and (b) ZB10f; (c) and (d) ZB20f. The surface normal to the applied pressure direction is shown.

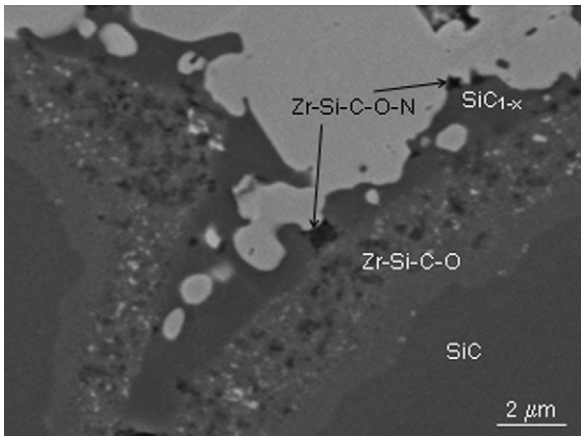

Fig. 7. SEM image showing the layered structure of the matrix/fiber interface.

Zr–Si phases at the triple points was assessed and the interface was disclosed to be constituted by ZrC nanocrystals embedded into a partially amorphous Si–C–O phase (Fig. 8). The fibers themselves showed a multilayered core–shell morphology: the inner part is constituted by stoichiometric SiC, the surrounding shell is amorphous Si–C–O with embedded ZrC nanocrystals and the outermost jagged layer is a Si–C phase with low C content. In fact, Hi Nicalon fibers are constituted by a polycarbosilane-derived amorphous/microcrystalline Si–C–O that suffers a degradation as it transforms to equilibrium products during exposure to high temperatures.[16]

Concerning the overall densification mechanisms, the following considerations can be stated. On the basis of thermodynamic calculations[17] for the system Zr–B–Si–O–N, ZrB_2 and Si_3N_4 phases cannot coexist under the process conditions. In fact, the occurring reactions lead to the complete disappearance of Si_3N_4 and produce various compounds (BN, ZrN, t-ZrO_2, $ZrSi_2$, amorphous B–N–O–Si–Zr). The steep increase in the densification rate at around 1560 °C (Fig. 1) is due to the formation of an eutectic liquid by reactions between the present phases. Starting from ZrB_2, Si_3N_4 and B_2O_3, during the heating up the main reaction occurring first could be the following:

$$2B_2O_3 + Si_3N_4 \rightarrow 4BN + 3SiO_2 \quad (1)$$

This reaction, characterized by a negative Gibbs free energy (−304 kJ/mol, at 1500 °C), describes the removal of the boron oxide present on the surface of the ZrB_2 particles. However, the liquid phase formed at about 1560 °C is probably due to the reaction among Si_3N_4, SiO_2 and ZrB_2. The formation of liquid Si is also favored but, in the final microstructure, only a residual borosilicate amorphous phase was found. Si-containing phases, i.e. $ZrSi_2$, were found at the triple junctions in the sintered materials, while the borosilicate compound was frequently detected as a secondary phase.

The addition of SiC whiskers and fibers introduced a further source of SiO_2 which in turn increased the amount of the liquid phase and decreased its viscosity. The higher volume of liquid phase with a lower viscosity, which should favor grain rearrangement and mass transport mechanisms, was very likely counterbalanced by the sterical impedance of the rod-shaped reinforcement. Hence, densification as well as grain growth of the matrix grains was not significantly altered compared to the baseline material.

The morphology of the fibers/matrix interface upon sintering induces to hypothesize that, as the temperature increases, the external part of the fibers, rich in oxygen, softens and incorporates ZrB_2 powder particles which are still free to move. A sketch of the presumed interaction mechanism among fiber, matrix and liquid phase, is shown in Fig. 9. The ZrB_2 particles may react with silica and the SiCO phase according to reaction (2):

$$ZrB_2 + SiCO + SiO_2 \rightarrow ZrC + B_2O_{3(l)} + 2Si_{(l)} \quad (2)$$

The liquid silicon formed is then squeezed out and reduced to SiC_{1-x} by the C-rich environment. The irregular morphology of this crest attests the solidification from a liquid phase (see Fig. 7). At the same time, once reached the melting temperature of the liquid phase in the matrix, constituted by the reaction products among Si_3N_4 and B_2O_3, the interaction and mass transfer between the two liquid phases are active and a strong chemical bonding is created upon cooling. The nitrogen peak detected by

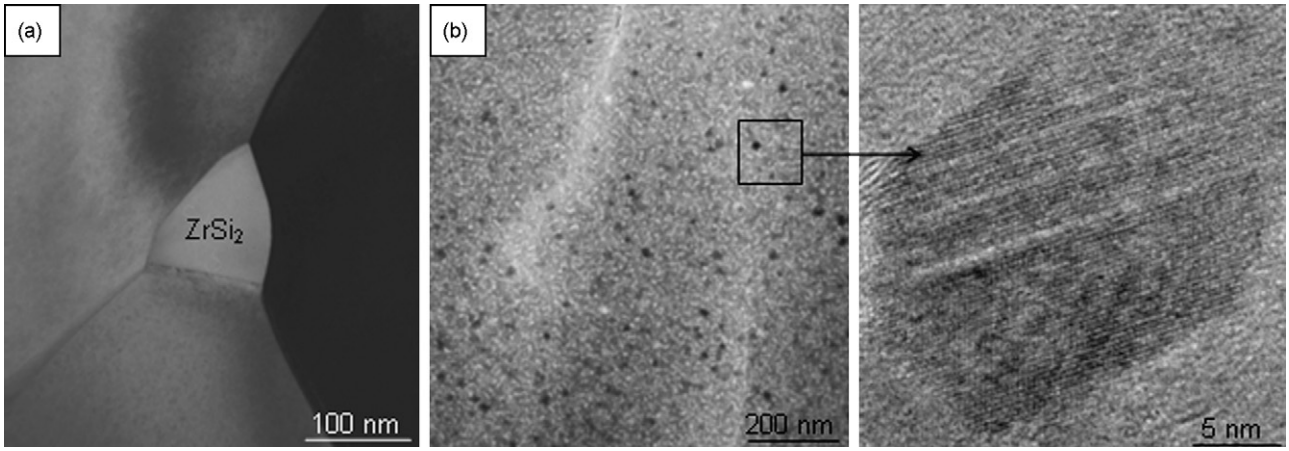

Fig. 8. TEM images showing (a) a triple point junction among ZrB_2 grains and (b) the nanocrystalline nature of the matrix/fiber interface, at the right a high-resolution image of a ZrC nanoparticle embedded into a Si–C–O amorphous phase.

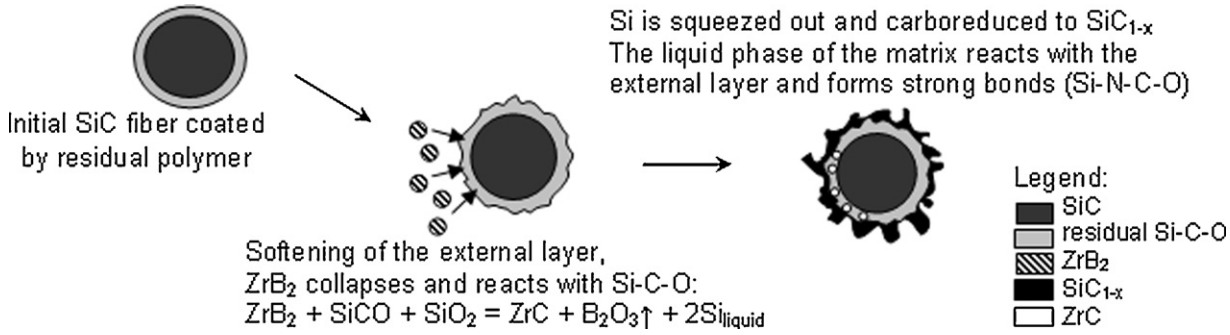

Fig. 9. Sketch of the possible interaction mechanism at high temperature among fiber, matrix and liquid phase.

Table 2
Mechanical properties of the baseline material and of the reinforced composites. HV1.0: Vickers hardness, K_{Ic}: fracture toughness, σ_{RT}: room-temperature flexural strength. σ_{1200}: flexural strength at 1200 °C. The Δvalues are referred to the ZB composite. The values are expressed as mean ± 1 standard deviation.

Sample	HV1.0[a] (GPa)	K_{Ic} (MPa m$^{1/2}$)	ΔK_{Ic} (%)	σ_{RT} (MPa)	$\Delta\sigma$ (%)	σ_{1200} (MPa)
ZB	13.4 ± 0.6	3.75 ± 0.10	–	600 ± 90	–	240 ± 30
ZB10w	13.3 ± 0.5	5.00 ± 0.09	+33	708 ± 35	+18	356 ± 37
ZB20w	9.5 ± 0.8	5.28 ± 0.33	+41	614 ± 75	=	352 ± 22
ZB10f	14.1 ± 0.6	5.32 ± 0.33	+42	389 ± 37	−35	409 ± 9
ZB20f	14.6 ± 0.3	5.65 ± 0.30	+52	413 ± 17	−31	335 ± 50

[a] Measured on the surface normal to the direction of the applied pressure.

EDS in the darkest region surrounding the core of the fibers is the proof of an intimate bonding between the liquid phase of the matrix and the fibers.

3.3. Mechanical properties

The mechanical properties of the ZrB_2-based composites are reported in Table 2, together with the relative variation compared to the baseline material.

The hardness was measured on surfaces perpendicular and parallel to the applied pressure and the highest values resulted those relative to the perpendicular surface; the average difference between the two values was between 10 and 15%. In the whisker-reinforced composites, ZB10w had a hardness of 13.3 GPa, similar to the baseline material, while the ZB20w composites showed the poorest value, 9.5 GPa, due to its low relative density. The highest values, above 14 GPa, were measured in the fiber-reinforced composites. Considering the data dispersion, in these composites the hardness did not significantly vary with the fibers content.

The fracture toughness increased from 3.75 MPa m$^{1/2}$ of the starting matrix to 5.0–5.7 MPa m$^{1/2}$ for the composites, indicating that some toughening phenomena occurred. The highest value (5.7 MPa m$^{1/2}$) was found for the ZB20f composite, which represents a toughness increase of more than 50% with respect to the matrix.

Example of crack paths generated by a 10-kg indentation in the composites are shown in Fig. 10a. In the whiskers-reinforced composites, very few whiskers were crossed by the crack front and the crack propagated mainly along the grain boundaries or at whisker/matrix interface. Occasionally, some crack branching also occurred. From what can be observed on the fracture surfaces and from the interaction between the crack front and the microstructure, in these whiskers-reinforced composites crack bridging and residual stresses could be the toughening mechanisms responsible of the increase of the fracture toughness. The contribution from the residual stress is taken into consideration due to the unavoidable mismatch between the thermal expansion coefficients and elastic constants of the matrix and whiskers. An attempt to quantitatively evaluate the overall contribution of these two mechanisms is shown in Fig. 11, see Appendix A for equations and input values.[18,19] The negative toughness contribution of the residual stress is due to the fact that the coefficient of thermal expansion of the SiC whiskers is lower than that of the matrix.[19,20] As can be seen, the agreement between theory and experiments is not very good. Deeper investigations are necessary to explore the effective toughening mechanisms which

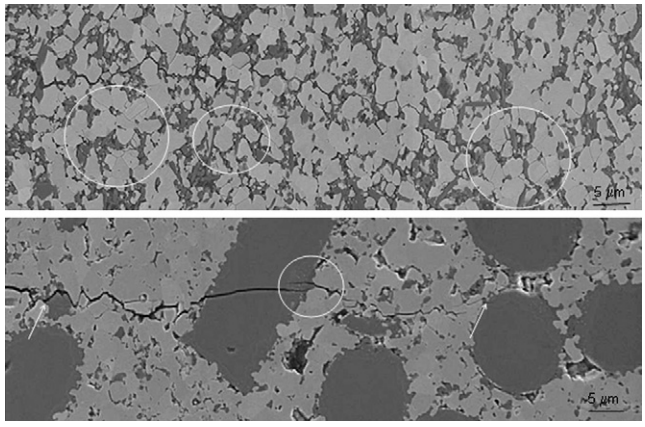

Fig. 10. Crack path generated by a 10-kg indentation in (a) ZB20w and (b) ZB20f. The cracks propagate from left to right. Note in (a) the microcracking in the circled areas. In (b) the arrows indicate the crack deflection around some fibers and the circled area evidences some bridging across the interface fiber–matrix.

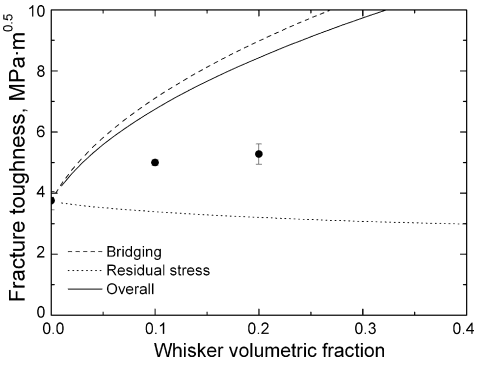

Fig. 11. Plot of the single and overall toughening contributions for the whiskers-reinforced composites. Experimental values are represented by points ± 1 standard deviation.

operate in this type of composites. However, the discrepancy could be rationalized keeping in mind that the original whiskers underwent a clear degradation so that the input values could be far different from the actual values. Moreover, the model usually considers an ideal reinforcement behavior while in real systems the effective in situ behavior should be considered.[21] For example, in most models the reinforcement active fraction is taken as the nominal reinforcement fraction and not as the effective active fraction. In our case, it was observed that the eventual bridging active fraction of the SiC whiskers is definitely lower than the nominal fraction (Fig. 3a and c). The estimate of the expected overall toughness shown in Fig. 11 can be therefore considered as a limiting potential target for this type of composites.

In the fiber-reinforced composites, the interaction of the crack front is shown in Fig. 10b. No pullout was observed and the crack mainly crossed the fibers maintaining its previous path. This is a consequence of the matrix/fiber interface which does not allow the debonding of the fiber and results in no pullout. From the above features and considering the high fracture strength of the fibers, crack pinning and residual stresses can be considered as the active toughening mechanisms in these composites. The comparison of the expected overall toughness and the experimental values is shown in Fig. 12, see Appendix A for equations and input values.[19,22] As it can be seen, in this case the agreement between theory and experiments is much better than for the whiskers-reinforced composites.

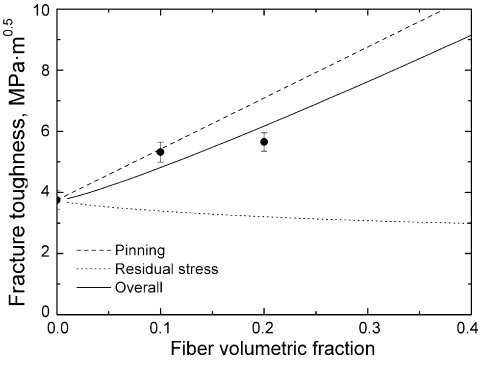

Fig. 12. Plot of the single and overall toughening contributions for the fibers-reinforced composites. Experimental values are represented by points ± 1 standard deviation.

The room-temperature flexural strength of the composite containing 10 vol.% of whiskers increased in comparison to baseline material. When the whiskers addition was 20 vol.%, the flexural strength of the composite was the same as for the baseline matrix (see Table 2). Fractographic analyses revealed that the critical flaws were mainly Zr–Si–N aggregates with a size of about 100 μm and not whiskers agglomerates.

In the fiber-reinforced composites, the room-temperature flexural strength decreased of about 30% compared to the baseline material, without any significant dependency on the fiber volumetric fraction (Table 2). No clear fracture origin could be identified on the fracture surfaces. Using the Griffith equation $\sigma = 1.3\,K_{Ic}/C^{1/2}$ the size of the mean critical defect (C) was estimated to be about 100 μm, which is of the same order of magnitude of the fibers dimension indicating that the fibers themselves can act as critical flaws. This could be particularly true when they were located at the surface of the bars. Being monocrystals with a low fracture toughness, the fibers could have been severely damaged by machining. The easy fracture propagation from the fibers into the matrix was then permitted by the strong fiber/matrix interface.

At high temperature, the SiC reinforcement effectively strengthened the composites notwithstanding the higher amount of intergranular glassy phase. In fact, the flexural strength at 1200 °C of the reinforced composites was higher than the baseline material in all the cases, with the highest value measured on the 10 vol.% fibers-reinforced composite (see Table 2).

4. Conclusions

ZrB_2-based materials reinforced with 10–20 vol.% SiC whiskers or SiC short fibers were hot-pressed at temperature between 1650 and 1730 °C. The addition of Si_3N_4 as sintering additive allowed achieving densities higher than 95% of the theoretical values.

Whiskers were observed to be very sensitive to the temperature and lost their original shape.

Fibers were more stable than whiskers, but a layered strong interface formed upon sintering. The core of the fibers was constituted by SiC, then a Si–C–O interlayer containing ZrC nanoparticles acted as a grab for the outermost jagged layer composed by SiC_{1-x} and Si–C–N phases. This graded structure of the fibers formed a very strong interface with the matrix and hindered any fiber pullout.

The fracture toughness increased of the 30 or 50% when 20 vol.% of SiC whiskers or fibers were added, respectively. The supposed active toughening mechanisms were residual stress and bridging in the case of whiskers-reinforced composites, and residual stress and crack pinning in the fibers-reinforced composites. The comparison between the experimental values and the expected toughness increment due to these mechanisms was good for the latter composites but not for the former. The room-temperature strength increased or remained unaltered for whiskers addition, but decreased of about 30% when the fibers were added. On the other hand, both whiskers and fibers strengthened the baseline material at high temperature.

This study pointed out that effective toughening and strengthening effects can be exercised by SiC whiskers or SiC short fibers. To fully exploit their potential, however, several conditions should be fulfilled. In the case of the whiskers-reinforced composites, the processing temperature must be kept lower than 1650 °C to avoid whiskers degradation. In the case of the fibers-reinforced composites, a weaker fiber/matrix interface should be obtained in order to promote a more effective toughening mechanism. At room-temperature, the fiber dimension seems to have a negative effect on strength.

Acknowledgements

The authors gratefully acknowledge the financial support of The Air Force Research Laboratory through the research grant FA8655-09-M-4002, in particular the contract monitor, Dr. Joan Fuller.

Daniele Dalle Fabbriche is acknowledged for hot-pressing cycles and Mathis Müller for his precious help in TEM specimens preparation.

Appendix A.

In this appendix, the equations and the input values used for calculating the toughening increment due to residual stress, crack bridging and crack pinning are reported.

A.1. Residual stress

The toughening increment, ΔK, due to residual stress is given by (3)[19]:

$$\Delta K = 2q\sqrt{\frac{2(\lambda - d)}{\pi}} \tag{3}$$

where λ is the interparticle distance, d is the mean size and q is the matrix residual stress given by (4):

$$q = \frac{-f_p\bar{\sigma}}{1 - f_p} \tag{4}$$

where f_p is the reinforcement volumetric fraction and $\bar{\sigma}$, in the case of fiber-shaped inclusion, is given by (5):

$$\bar{\sigma} = \frac{2\sigma_{11} + \sigma_{33}}{3} \tag{5}$$

For fiber-shaped inclusion, the principal thermal residual stresses are: σ_{33} acting along the axis of the fiber-shaped inclusion, and σ_{11} and σ_{22} on the plane perpendicular to this axis. Their expression reads as follows in (6) and (7)[18]:

$$\sigma_{11} = \sigma_{22} = A\left\{\left[\frac{1}{E_p} + \frac{f_p}{(1 - f_p)E_m}\right](\alpha_m - \alpha_1) + \left[\frac{\nu_p}{E_p} + \frac{f_p\nu_m}{(1 - f_p)E_m}\right](\alpha_m - \alpha_3)\right\}\Delta T \tag{6}$$

$$\sigma_{33} = A\left\{2\left[\frac{\nu_p}{E_p} + \frac{f_p\nu_m}{(1 - f_p)E_m}\right](\alpha_m - \alpha_1) + \left[\frac{1 - \nu_p}{E_p} + \frac{1 + f_p + (1 - f_p)\nu_m}{(1 - f_p)E_m}\right](\alpha_m - \alpha_3)\right\}\Delta T \tag{7}$$

with

$$A = \left[\frac{(1 + \nu_p)(1 - 2\nu_p)}{E_p^2} + \frac{f_p(2 - \nu_p - \nu_m - 4\nu_p\nu_m) + 1 + \nu_m}{(1 - f_p)E_pE_m} + \frac{f_p(1 + \nu_p)(1 + f_p - 2f_p\nu_m)}{(1 - f_p)^2E_m^2)}\right]^{-1} \tag{8}$$

E_p, E_m, ν_p and ν_m are the Young's modulus and the Poisson ratio of the inclusion and matrix, respectively; α_1, α_2 (=α_1) and α_3 are the coefficient of linear expansion (CTE) of the fiber-shaped inclusion in the three directions and α_m is the CTE of the matrix.

The interparticle distance was taken as[19]

$$\lambda = \frac{1.085d}{\sqrt{f_p}} \tag{9}$$

In this first approximation, the mean reinforcement size, d, was evaluated by a commercial image analysis software and resulted to be 6.6 μm and 18 μm for the whiskers-reinforced and fibers-reinforced composites, respectively. In the case of the whiskers, the input values for E_p, E_m, ν_p, e ν_m, were 352 GPa, 419 GPa, 0.21[18] and 0.12. Since the thermal expansion of the β-SiC whiskers is isotropic,[18] a common value of 4.45×10^{-6}/°C was taken for the α_i, the corresponding value for the matrix, α_m, was 6.20×10^{-6}/°C. In the case of the fibers, E_p and ν_p were taken as 400 GPa and 0.17, respectively,[23] while all the other values were the same of the whiskers. Irrespective of the type of reinforcement, for ΔT a stress-free temperature of −1000 °C was considered.

A.2. Bridging

The toughening increment, ΔK, due to whisker bridging is given by (10)[18]:

$$\Delta K_I = \frac{\{[(K^m)^2 + 2(\sigma_f^w)^2 f_p r E_c G^m/3(1 - \nu_m^2)E^w G^i]^{1/2} - K^m\}}{2} \tag{10}$$

where K^m is the matrix fracture toughness, σ_f^w is the whiskers fracture strength (10 GPa),[18] r is the whisker radius (0.5 μm) and E_c is the composite Young's modulus, which was calculated according to the rule of mixture. The other symbols have the same meaning as above. The ratio G^m/G^i was taken as 24.[18]

A.3. Crack pinning

The toughening increment, ΔK, due to crack pinning is given by (11)[22]:

$$\Delta K = 2\sqrt{\frac{4r}{\pi}}f_p\sigma_p \tag{11}$$

where r is the radius of the reinforcement and σ_p its fracture strength of the reinforcement. For the fibers, they were taken as 7.5 μm and 2.7 GPa,[24] respectively.

References

1. Chamberlain AL, Fahrenholtz WG, Hilmas GE, Ellerby DT. High strength ZrB_2-based ceramics. *J Am Ceram Soc* 2004;**87**:1170–2.
2. Opeka MM, Talmy IG, Wuchina EJ, Zaykoski JA, Causey SJ. Mechanical, thermal, and oxidation properties of hafnium and zirconium compounds. *J Eur Ceram Soc* 1999;**19**:2405–14.
3. Chamberlain AL, Fahrenholtz WG, Hilmas GE, Ellerby DT. In: Bansal NP, Singh JP, Kriven WM, Schneider H, editors. *Characterization of zirconium diboride–molybdenum disilicide ceramics. In ceramic transactions, vol. 153. Advances in ceramic matrix composites IX*. Westerville, OH: Am. Ceram. Soc.; 2003. pp. 299–308.
4. Rezaie A, Fahrenholtz WG, Hilmas GE. Effect of hot pressing time and temperature on the microstructure and mechanical properties of ZrB_2–SiC. *J Mater Sci* 2007;**42**:2735–44.
5. Silvestroni L, Sciti D. Effects of $MoSi_2$ additions on the properties of Hf– and Zr–B_2 composites produced by pressureless sintering. *Scripta Mater* 2007;**57**:165–8.
6. Wang H, Wang CA, Yao X, Fang D. Processing and mechanical properties of zirconium diboride-based ceramics prepared by spark plasma sintering. *J Am Ceram Soc* 2007;**90**:1992–7.
7. Zhang P, Hu P, Zhang X, Han J, Meng S. Processing and characterization of ZrB_2–SiCw ultra-high temperature ceramics. *J Alloys Compd* 2009;**20**:358–62.
8. Zhang X, Xu L, Du S, Han J, Hu P, Han W. Fabrication and mechanical properties of ZrB_2–SiCw ceramic matrix composite. *Mater Lett* 2008;**62**:1058–60.
9. Yang F, Zhang X, Han J, Du S. Processing and mechanical properties of short carbon fibers toughened zirconium diboride-based ceramics. *Mater Design* 2008;**29**:1817–20.
10. Tian WB, Kan Y-M, Zhang G-J, Wang P-L. Effect of carbon nanotubes on the properties of ZrB_2–SiC ceramics. *Mater Sci Eng A* 2008;**487**:568–73.
11. Wang Z, Dong S, Zhang X, Zhou H, Wu D, Zhou Q, Jiang D. Fabrication and properties of C_f/SiC–ZrC composites. *J Am Ceram Soc* 2008;**91**:3434–6.
12. Balbo A, Sciti D. Spark plasma sintering and hot pressing of ZrB2–MoSi2 ultra-high-temperature ceramics. *Mat Sci Eng A* 2008;**475**:108–12.
13. Munz DG, Shannon Jr JL, Bubsey RT. Fracture toughness calculations from maximum load in four point bend tests of chevron notch specimens. *Int J Fract* 1980;**16**:R137–41.
14. Monteverde F, Bellosi A. Effect of the addition of silicon nitride on sintering behaviour and microstructure of zirconium diboride. *Scripta Mater* 2002;**46**:223–8.
15. Monteverde F, Guicciardi S, Bellosi A. Advances in microstructure and mechanical properties of zirconium diboride based ceramics. *Mater Sci Eng A* 2003;**346**:310–9.
16. Kerans RJ, Hay RS, Pagano NJ. The role of the fiber–matrix interface in ceramic composites. *Ceram Bull* 1989;**68**:429–42.
17. Roine A. HSC Chemistry for Windows 5, Outukumpu Research Oy Pori, Finland.
18. Becher PF, Hsueh C-H, Angelini P, Tiegs TN. Toughening behavior in whisker-reinforced ceramic matrix composites. *J Am Ceram Soc* 1988;**71**:1050–61.
19. Taya M, Hayashi S, Kobayashi AS, Yoon HS. Toughening of a particulate-reinforced ceramic–matrix composite by thermal residual stress. *J Am Ceram Soc* 1990;**73**:1382–91.
20. Cutler RA. Engineering properties of borides. In: Schneider Jr SJ, editor. *Engineered materials handbook*, vol. 4. ASM International; 1991. p. 787–803.
21. Sciti D, Celotti G, Pezzotti G, Guicciardi S. On the toughening mechanisms of $MoSi_2$ reinforced Si_3N_4 ceramics. *Appl Phys A* 2007;**86**: 243–8.
22. Rouxel T, Laurent Y. Fracture characteristics of SiC particle reinforced oxynitride glass using chevron-notch three-point bend specimens. *Int J Fract* 1998;**91**:83–101.
23. Guo SQ, Kagawa Y. Characterization of interface sliding damage in SiC fiber-reinforced Ti-15-3 matrix composite by cyclic fatigue. *Acta Mater* 1997;**45**:2257–70.
24. COI Ceramics, Ceramics Matrix Composites, Specialty Ceramics & Fibers. Magna, UT, USA, Lot Certification Sheet.